

# Conformational properties of 1-fluoro-1-methyl-silacyclohexane and 1-methyl-1-trifluoromethyl-1-silacyclohexane: Gas electron diffraction, low-temperature NMR, temperature-dependent Raman spectroscopy, and quantum chemical calculations<sup>☆</sup>

Sunna Ó. Wallevik<sup>a,1</sup>, Ragnar Bjornsson<sup>a,2</sup>, Ágúst Kvaran<sup>a</sup>, Sigridur Jonsdottir<sup>a</sup>, Georgiy V. Girichev<sup>b</sup>, Nina I. Giricheva<sup>c</sup>, Karl Hassler<sup>d</sup>, Ingvar Arnason<sup>a,\*</sup>

<sup>a</sup> Science Institute, University of Iceland, Dunhaga 3, IS-107 Reykjavik, Iceland

<sup>b</sup> Ivanovo State University of Chemistry and Technology, Ivanovo 153460, Russia

<sup>c</sup> Ivanovo State University, Ivanovo 153025, Russia

<sup>d</sup> Institut für Anorganische Chemie, Technische Universität Graz, Stremayergasse 16, A-8010 Graz, Austria

## ARTICLE INFO

### Article history:

Received 1 December 2009

Received in revised form 19 February 2010

Accepted 22 February 2010

Available online 1 March 2010

This work is dedicated to Prof. Heinz Oberhammer on the occasion of his 70th birthday

### Keywords:

Conformational analysis  
Gas electron diffraction  
Low-temperature NMR  
Temperature-dependent Raman spectroscopy  
Quantum chemical calculations  
Substituent effects

## ABSTRACT

Two new 1,1-disubstituted silacyclohexanes, C<sub>5</sub>H<sub>10</sub>SiFCH<sub>3</sub> (**1**) and C<sub>5</sub>H<sub>10</sub>SiCF<sub>3</sub>CH<sub>3</sub> (**2**) were synthesized. The molecular structure of their axial and equatorial conformers as well as the thermodynamic equilibrium between these species was investigated by means of gas electron diffraction (GED), dynamic nuclear magnetic resonance (DNMR), temperature-dependent Raman spectroscopy, and quantum chemical calculations (CCSD(T), MP2, and DFT methods). **1a**, **2a** and **1e**, **2e** are used to denote the conformers having the CH<sub>3</sub> group in axial and equatorial positions, respectively. According to GED, both compounds exist as a mixture of two conformers possessing the chair conformation of the six-membered ring and C<sub>3</sub> symmetry and differing in the axial or equatorial position of the two substituents (axial-CH<sub>3</sub>:equatorial-CH<sub>3</sub> ratio of 45(6%):55(6)% and 51(5%):49(5)% was found for **1** and **2**, respectively). Hence, G<sub>ax</sub>–G<sub>eq</sub> = 0.11(13) kcal mol<sup>-1</sup> for **1**, whereas **2a** and **2e** have virtually the same free energy. Low-temperature <sup>19</sup>F NMR experiments resulted in G<sub>ax</sub>–G<sub>eq</sub> = 0.26(2) kcal mol<sup>-1</sup> at 125 K for **1** and G<sub>ax</sub>–G<sub>eq</sub> = 0.36(2) kcal mol<sup>-1</sup> at 118 K for **2**. Temperature-dependent Raman spectroscopy in the temperature range of 210–300 K of the neat liquids and their solutions in THF and hexane indicates that **1e** and **2e** are favoured over **1a** and **2a** by 0.50(15) and 0.73(15) kcal mol<sup>-1</sup>, respectively (Δ*H* values). The Raman results seem not to depend on the polarity of the medium. CCSD(T)/CBS calculations at the NMR temperatures predict G<sub>ax</sub>–G<sub>eq</sub> = 0.28 and 0.36 kcal mol<sup>-1</sup> for **1** and **2**, respectively, and are thus in excellent agreement with the DNMR results. The agreement of CCSD(T)/CBS with the GED results is slightly worse, predicting G<sub>ax</sub>–G<sub>eq</sub> = 0.31 and 0.22 kcal mol<sup>-1</sup> for **1** and **2**, respectively. The CCSD(T)/CBS calculations are also in slight disagreement with the Raman results, predicting Δ*H* values of 0.25 and 0.48 kcal mol<sup>-1</sup> for **1** and **2**, respectively. The CCSD(T)/CBS calculations of both mono- and disubstituted silacyclohexanes with F, CH<sub>3</sub>, and CF<sub>3</sub> substituents revealed a remarkable good additivity of substituent effects, which is not shown by the analogous cyclohexanes.

© 2010 Elsevier B.V. All rights reserved.

## 1. Introduction

The stereochemistry of cyclohexane and monosubstituted cyclohexanes is among the best explored areas in organic stereo-

chemistry [2,3]. As a rule the substituent prefers the equatorial position of the chair conformation, when the substituent becomes bulkier its equatorial preference generally increases. Winstein and Holness defined *A* values as the thermodynamic preference for the equatorial conformation over the axial one (see Scheme 1 for definition of *A*) [4]. A positive *A* value corresponds to a preference for the equatorial conformer and Δ*G* = G<sub>ax</sub>–G<sub>eq</sub>. All energy differences herein will be presented as (axial–equatorial). The chair-to-chair inversion is well understood, in cyclohexane the Gibbs free energy of activation for the step chair → half-chair<sup>#</sup> → twist is generally accepted to be 10.1–10.5 kcal mol<sup>-1</sup>. Far less investigations

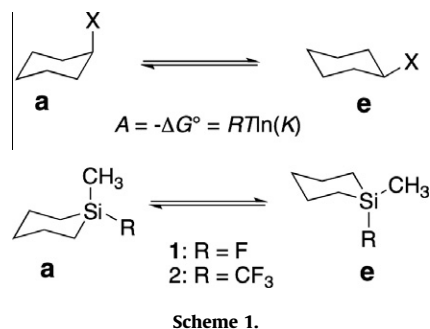
<sup>☆</sup> Conformation of Silicon-Containing Rings, 9. For Part 8 see Ref. [1].

\* Corresponding author.

E-mail address: [ingvara@raunvis.hi.is](mailto:ingvara@raunvis.hi.is) (I. Arnason).

<sup>1</sup> ICI Rheocenter, Keldnaholti, IS-112 Reykjavik, Iceland.

<sup>2</sup> School of Chemistry, North Haugh, University of St. Andrews, St. Andrews, Fife KY16 9ST, UK.



have been reported on silacyclohexane and its derivatives. In silacyclohexane the activation energy is about one-half of the value for cyclohexane [5,6]. In recent years we have reported on the conformational properties of monosubstituted silacyclohexanes, with  $\text{CH}_3$  [7],  $\text{CF}_3$  [8,9], F [10], and  $\text{SiH}_3$  [1] as substituents.

In Table 1 the conformational properties of these four monosubstituted silacyclohexanes are presented and compared to available data for the analogous cyclohexanes.

It is striking to see how different these two, so close related, ring systems behave. Not only is the overall equatorial preference of the cyclohexanes greatly diminished in methylsilacyclohexane, moreover is the overwhelming equatorial preference of trifluoromethylcyclohexane turned upside down in trifluoromethylsilacyclohexane. The fluoro- and silylsilacyclohexane also show a very different behaviour when compared with corresponding cyclohexanes.

Additivity of conformational energies in di- or polysubstituted six-membered ring systems has been subject to considerable research [3]. In geminally disubstituted cyclohexanes, additivity of conformational energies tends to break down. This has been explained by altered rotameric preference of one substituent by the other substituent [17]. A well-known example is 1-methyl-1-phenylcyclohexane. By addition of  $A$  values the conformer with methyl axial and phenyl equatorial is predicted to be stabilized by  $1.1 \text{ kcal mol}^{-1}$ . Experimentally, the inverted conformer (phenyl axial) was found to be favoured by  $0.3 \text{ kcal mol}^{-1}$  [17,18]. Nonetheless, we were interested in seeing to what degree 1,1-disubstituted-1-silacyclohexanes might show addition of conformational properties. For two reasons, one might expect some additional effect to appear. First, the substituents we have used so far are

not bulky, and second, compared to carbon the silicon atom is larger and forms longer bonds to the substituent as well as to the neighbouring carbon ring atoms. Therefore, a hindered rotation of one substituent by the other or by ring hydrogen atoms is not likely to play a major role in the conformational behaviour of geminally disubstituted silacyclohexanes as long as non-bulky substituents are used. On the other hand, absence of conformational additivity by the substituents would indicate that other explanations must be called into play. Herein we report on the conformational properties of 1-fluoro-1-methyl-1-silacyclohexane **1** and 1-methyl-1-trifluoromethyl-1-silacyclohexane **2** (Scheme 1) using gas electron diffraction (GED), low-temperature NMR, temperature-dependent Raman spectroscopy, and quantum chemical calculations.

## 2. Experimental

### 2.1. General

All solvents were dried using appropriate drying agents and distilled prior to use. Standard Schlenk technique was used for all manipulations. Antimony trifluoride was dried by continuous heating under vacuum for three days prior to use. Chloromethylsilacyclohexane was prepared as described by West [19].

### 2.2. 1-Fluoro-1-methyl-1-silacyclohexane (**1**)

Antimony trifluoride (2.2 g, 12.2 mmol) was transferred into a 70 mL Schlenk tube containing chloromethylsilacyclohexane (3.7 g, 25.2 mmol). The reaction mixture was stirred at  $0^\circ\text{C}$  for 2 h, with the solution soon turning red and then dark brown. The ice bath was allowed to warm up to room temperature and the solution was stirred overnight. The product was then condensed into a trap held at  $-196^\circ\text{C}$ , resulting in a colourless liquid. Further purification was achieved by the use of preparative GC, attaining an analytically pure substance. Yield: 2.99 g (22.6 mmol, 90%).  $^1\text{H}$  NMR (400 MHz,  $\text{CDCl}_3$ ):  $\delta = 0.22$  (d,  $^3J_{\text{H-F}} = 7.4 \text{ Hz}$ , 3H,  $\text{CH}_3$ ), 0.58–0.68 (m, 2H,  $\text{CH}_{2(\text{ax/eq})}$ ), 0.83–0.90 (m, 2H,  $\text{CH}_{2(\text{ax/eq})}$ ), 1.30–1.39 (m, 1H,  $\text{CH}_{2(\text{ax/eq})}$ ), 1.47–1.56 (m, 1H,  $\text{CH}_{2(\text{ax/eq})}$ ), 1.68–1.76 (m, 4H,  $\text{CH}_2$ ).  $^{13}\text{C}$  NMR (101 MHz,  $\text{CDCl}_3$ ):  $\delta = -2.6$  (d,  $\text{CH}_3$ ,  $^2J_{\text{F-C}} = 14.8 \text{ Hz}$ ), 14.6 (d,  $\text{CH}_2$ ,  $^2J_{\text{F-C}} = 12.7 \text{ Hz}$ ), 24.0, 29.5 ( $\text{CH}_2$ );  $^{19}\text{F}$  NMR (376 MHz,  $\text{CDCl}_3$ ):  $\delta = -168.4$  to  $(-168.5)$  (m,  $^3J_{\text{H-F}} = 7.4 \text{ Hz}$ ,  $^1J_{\text{Si-F}} = 286 \text{ Hz}$ ).

**Table 1**  
Conformational properties of selected monosubstituted silacyclohexanes and cyclohexanes. All values are in  $\text{kcal mol}^{-1}$  and are given as (axial–equatorial).

	GED	NMR	Raman	QC <sup>f</sup>		GED	NMR	Raman	QC <sup>f</sup>
	$A$	$A$	$\Delta H$	$\Delta E$		$A$	$\Delta H$	$\Delta E$	
X = $\text{CH}_3$	0.45 <sup>a</sup>	0.23 <sup>a</sup>	0.15 <sup>e</sup>	0.12 <sup>g</sup>	X = $\text{CH}_3$	1.9 <sup>h</sup>	1.6 <sup>k</sup>	i	1.70 <sup>g</sup>
X = $\text{CF}_3$	-0.19 <sup>b</sup>	-0.4 <sup>b</sup>	-0.5 <sup>e</sup>	-0.50 <sup>g</sup>	X = $\text{CF}_3$	i	2.37 <sup>l</sup>	i	2.26 <sup>g</sup>
X = F	-0.31 <sup>c</sup>	-0.13 <sup>c</sup>	-0.25 <sup>c</sup>	-0.15 <sup>g</sup>	X = F	0.16 <sup>j</sup>	0.35 <sup>k</sup>	i	0.12 <sup>g</sup>
X = $\text{SiH}_3$	-0.17 <sup>d</sup>	0.05 <sup>d</sup>	-0.26 <sup>d</sup>	-0.14 <sup>g</sup>	X = $\text{SiH}_3$	i	1.45 <sup>k</sup>	1.49 <sup>m</sup>	1.26 <sup>g</sup>

<sup>a</sup> Ref. [7].

<sup>b</sup> Refs. [8,9].

<sup>c</sup> Ref. [10].

<sup>d</sup> Ref. [1].

<sup>e</sup> Ref. [11].

<sup>f</sup> QC = quantum chemical calculations.

<sup>g</sup> Ref. [12].

<sup>h</sup> Ref. [13].

<sup>i</sup> Not available.

<sup>j</sup> Ref. [14].

<sup>k</sup> Ref. [2].

<sup>l</sup> Ref. [15].

<sup>m</sup> Ref. [16].

$^{29}\text{Si}$  NMR (79 MHz,  $\text{CDCl}_3$ ):  $\delta = 27.5$  (d,  $^1J_{\text{Si-F}} = 286$  Hz). MS (EI, 70 eV):  $m/z$  (%) 132 (100), 89 (98).

### 2.3. 1-Trifluoromethyl-1-methyl-1-silacyclohexane (2)

$\text{CF}_3\text{Br}$  (13.2 g, 88.9 mmol) was condensed into a reaction flask containing chloromethylsilacyclohexane (10.0 g, 67.3 mmol) and  $\text{CH}_2\text{Cl}_2$  (30 mL). A  $-78^\circ\text{C}$  cooling bath (acetone/dry ice) was placed under the reaction flask and when the content of the flask had reached the temperature of the bath, a solution of  $\text{P}(\text{NEt}_2)_3$  (16.6 g, 67.3 mmol) in  $\text{CH}_2\text{Cl}_2$  (20 mL) was slowly added while stirring. The cooling bath was removed and after continued stirring at room temperature overnight, the colourless solution had turned orange. All volatile components were then condensed on an  $\text{N}_2(1)$  cooled finger. The solvent was distilled off and the product was collected by distillation under nitrogen at  $130^\circ\text{C}$ . Yield: 8.92 g, 73%.  $^1\text{H}$  NMR (400 MHz,  $\text{CDCl}_3$ ):  $\delta = 0.25$  (s, 3H,  $\text{CH}_3$ ), 0.66–0.73 (m, 2H,  $\text{CH}_{2(\text{ax/eq})}$ ), 0.97–1.03 (m, 2H,  $\text{CH}_{2(\text{ax/eq})}$ ), 1.28–1.38 (m, 1H,  $\text{CH}_{2(\text{ax/eq})}$ ), 1.51–1.60 (m, 1H,  $\text{CH}_{2(\text{ax/eq})}$ ), 1.67–1.83 (m, 4H,  $\text{CH}_2$ ).  $^{13}\text{C}$  NMR (101 MHz,  $\text{CDCl}_3$ ):  $\delta = -7.1$  (d,  $\text{CH}_3$ ,  $^3J_{\text{F-C}} = 1.3$  Hz), 9.3 (d,  $\text{CH}_2$ ,  $^3J_{\text{F-C}} = 1.3$  Hz), 23.5, 29.1 ( $\text{CH}_2$ ), 131.9 (q,  $\text{CF}_3$ ,  $^1J_{\text{C-F}} = 323$  Hz).  $^{19}\text{F}$  NMR (376 MHz,  $\text{CDCl}_3$ ):  $\delta = -65.4$  (s,  $^2J_{\text{Si-F}} = 36$  Hz).  $^{29}\text{Si}$  NMR (79 MHz,  $\text{CDCl}_3$ ):  $\delta = -1.5$  (d,  $^2J_{\text{Si-F}} = 36$  Hz). MS (EI, 70 eV):  $m/z$  (%) 182 (3), 113 (100), 85 (100). HRMS:  $m/z$  calcd for  $\text{C}_6\text{H}_{13}\text{Si}$  (M- $\text{CF}_3$ ) 113.0787, found 113.0769.

### 2.4. GED experiment

The electron diffraction patterns were recorded by the apparatus described previously [20,21] at two nozzle-to-plate distances (338 and 598 mm). The direct inlet system into the effusion cell with a cylindrical nozzle of  $0.6 \times 1.0$  mm size (diameter  $\times$  length) was used. The temperature of the effusion cell was kept at  $9(3)^\circ\text{C}$  and  $-11(3)^\circ\text{C}$  for  $\text{C}_5\text{H}_{10}\text{SiFCH}_3$  and  $\text{C}_5\text{H}_{10}\text{SiCH}_3\text{CF}_3$ , respectively. The main conditions of the combined gas electron diffraction and mass spectrometric experiments (GED/MS) are shown in Tables 2 and 3.

The mass spectra of the vapours under investigation were recorded simultaneously with the diffraction patterns and are given in Table 3. The heaviest detected ion for both studied compounds was the monomeric parent ion. For  $\text{C}_5\text{H}_{10}\text{SiFCH}_3$  the ions  $[\text{C}_4\text{H}_9\text{SiF}]^+$ ,  $[\text{C}_3\text{H}_7\text{SiF}]^+$ , and  $[\text{C}_2\text{H}_5\text{SiF}]^+$  connected with losing of two, three, and four  $\text{CH}_2$  groups, have highest intensities as well as the ion  $[\text{SiF}]^+$ . For the compound  $\text{C}_5\text{H}_{10}\text{SiCH}_3\text{CF}_3$  the mostly intensive ions have the stoichiometry  $[\text{C}_6\text{H}_{13}\text{Si}]^+$  and  $[\text{C}_4\text{H}_9\text{Si}]^+$ . The observed ions prove the absence of any detectable amount of volatile impurities in the samples.

The temperature of the effusion cell was measured by a W/Re-5/20 thermocouple that was calibrated at the melting points of Sn and Al. The electron wavelength was obtained by polycrystalline ZnO. The electron image Kodak films were used for the registration of the diffraction patterns. The optical densities were measured by a computer controlled MD-100 microdensitometer [22].

**Table 2**

Conditions of the simultaneous GED/MS experiments.

	$\text{C}_5\text{H}_{10}\text{SiFCH}_3$ (1)		$\text{C}_5\text{H}_{10}\text{SiCH}_3\text{CF}_3$ (2)	
Nozzle-to-plate distance (mm)	338	598	338	598
Fast electrons beam ( $\mu\text{A}$ )	1.4	0.65	1.02	0.77
Accelerating voltage (kV)	72	69	81	78
Temperature of effusion cell ( $^\circ\text{C}$ )	9(3)	9(3)	-12(3)	-10(3)
Ionization voltage (V)	50	50	45	45
Exposure time (s)	90	55	90	55
Residual gas pressure (Torr)	$2 \times 10^{-6}$	$3 \times 10^{-6}$	$1.5 \times 110^{-6}$	$3.7 \times 10^{-6}$

**Table 3**

Mass spectra recorded during the electron diffraction experiment.

$\text{C}_5\text{H}_{10}\text{SiFCH}_3$ (1)			$\text{C}_5\text{H}_{10}\text{SiCH}_3\text{CF}_3$ (2)		
$U_{\text{ioniz}} = 50$ V			$U_{\text{ioniz}} = 45$ V		
Ion	$m/e$	Abundance	Ion	$m/e$	Abundance
$[\text{C}_6\text{H}_{13}\text{SiF}]^+$	132	67	$[\text{C}_7\text{H}_{13}\text{SiF}_3]^+$	182	2
$[\text{C}_5\text{H}_{11}\text{SiF}]^+$	118	38	$[\text{C}_6\text{H}_{13}\text{Si}]^+$	113	100
$[\text{C}_4\text{H}_9\text{SiF}]^+$	103	84	$[\text{C}_4\text{H}_9\text{SiF}]^+$	103	5
$[\text{C}_4\text{H}_7\text{SiF}]^+$	102	12	$[\text{C}_3\text{H}_7\text{SiF}]^+$	89	10
$[\text{C}_3\text{H}_9\text{SiF}]^+$	92	31	$[\text{C}_4\text{H}_9\text{Si}]^+$	85	78
$[\text{C}_3\text{H}_7\text{SiF}]^+$	90	97	$[\text{CH}_3\text{SiF}_2]^+$	81	25
$[\text{C}_2\text{H}_6\text{SiF}]^+$	77	30	$[\text{C}_2\text{H}_5\text{SiF}]^+$	76	8
$[\text{C}_2\text{H}_5\text{SiF}]^+$	76	100	$[\text{CH}_4\text{SiF}]^+$	63	19
$[\text{CH}_4\text{SiF}]^+$	63	73	$[\text{C}_2\text{H}_7\text{Si}]^+$	59	19
$[\text{CH}_3\text{SiF}]^+$	62	26	$[\text{C}_2\text{H}_4\text{Si}]^+$	56	5
$[\text{H}_2\text{SiF}]^+$	49	14	$[\text{SiF}]^+$	47	18
$[\text{SiF}]^+$	47	92	$[\text{CH}_3\text{Si}]^+$	43	9
			$[\text{C}_3\text{H}_5]^+$	41	7

The background functions  $G(s)$  for the intensities  $I(s)$  of the long and short camera distances were approximated by smooth lines. Analysis of the first and second order derivatives of the  $G(s)$  functions was used to make sure that the oscillation of  $G(s)$ , which could be close to the oscillations of the  $sM(s)$  function, was absent. No elimination of high-frequency oscillations was done.

The molecular intensities  $sM(s)$  of  $\text{C}_5\text{H}_{10}\text{SiFCH}_3$  were obtained in the ranges  $2.2\text{--}26.9 \text{ \AA}^{-1}$  and  $1.1\text{--}15.0 \text{ \AA}^{-1}$  for the short and long camera distances, respectively. The molecular intensities  $sM(s)$  of  $\text{C}_5\text{H}_{10}\text{SiCH}_3\text{CF}_3$  were obtained in the ranges  $2.4\text{--}28.6 \text{ \AA}^{-1}$  and  $1.3\text{--}15.9 \text{ \AA}^{-1}$ , respectively. Figures showing the molecular intensities are available as [Supplementary Material](#).

### 2.5. Low-temperature NMR experiment

A solvent mixture of  $\text{CD}_2\text{Cl}_2$ ,  $\text{CH}_2\text{Cl}_2$ , and  $\text{CHF}_2\text{Cl}$  in a ratio of 1:1:3 was used for the low-temperature  $^{19}\text{F}$  NMR measurements (Bruker AC 250 Spectrometer). The temperature of the probe was calibrated by means of a type K (Chromel/Alumel) thermocouple inserted into a dummy tube the day before and the day after the NMR experiment. The readings are estimated to be accurate within  $\pm 2$  K. The NMR spectra were loaded into the data-handling program IGOR (WaveMetrics) for analysis, manipulations, and graphic display. Lorentzian line shape simulations of the NMR spectra were performed by using the WinDNMR program [23] to derive parameters relevant to conformational equilibria and rates of exchanges.

### 2.6. Low-temperature Raman experiment

Raman spectra were recorded with a Jobin Yvon T64000 spectrometer equipped with a triple monochromator and a CCD camera. The samples were filled into 1 mm capillary glass tubes and irradiated by the green 532 nm line of a frequency doubled Nd:YAG Laser (Coherent, DPSS model 532-20, 10 mW). Spectra were recorded from pure compound and in hexane and THF solution. A continuous flow cryostat, Oxford instruments OptistatCF<sup>TM</sup>,

using liquid nitrogen for cooling was employed for the low-temperature measurements.

## 2.7. Computational details

Calculations were performed with Gaussian 03 [24] and 09 [25] versions (DFT calculations and MP2/6-31G\*\*) and Molpro 2006.1 [26] (single-point MP2 and CCSD(T) calculations). Geometries of the axial and equatorial conformers (according to the position of the CH<sub>3</sub> group) of C<sub>5</sub>H<sub>10</sub>SiFCH<sub>3</sub> (Fig. 1) and C<sub>5</sub>H<sub>10</sub>SiCH<sub>3</sub>CF<sub>3</sub> (Fig. 2) were optimized with B3LYP/6-31G\*\* and MP2/6-31G\*\* and used to guide the GED analysis. The calculated geometric parameters of the axial form are listed in Tables 5 and 6 together with the experimental data.

<sup>19</sup>F chemical shifts were calculated with the GIAO [27,28] method for the axial and equatorial conformers of **1** and **2** in order to identify peaks in the low-temperature NMR spectra. These calculations were done with the PBE1PBE [29] functional, known to predict shielding constants well [30], with a basis set optimized for shielding constants, aug-pcS-2 [31] using geometries at the M06-2X/pc-2 level. CFCI<sub>3</sub> was used as a <sup>19</sup>F reference standard to obtain relative chemical shifts.

DFT calculations with the M06-2X functional [32,33] and the pc-2 basis set [34,35] (triple-zeta quality) were performed to explore the conformational energy surface of both molecules. The minimum energy pathways for the chair-to-chair inversion were calculated in redundant internal coordinates with the STQN method [36] as implemented in Gaussian 09 [25]. The path was calculated in four slices using the keyword OPT(QST3, PATH = 11).

In order to obtain accurate theoretical estimates of the axial/equatorial electronic energy difference,  $\Delta E$ , of **1** and **2**, single point

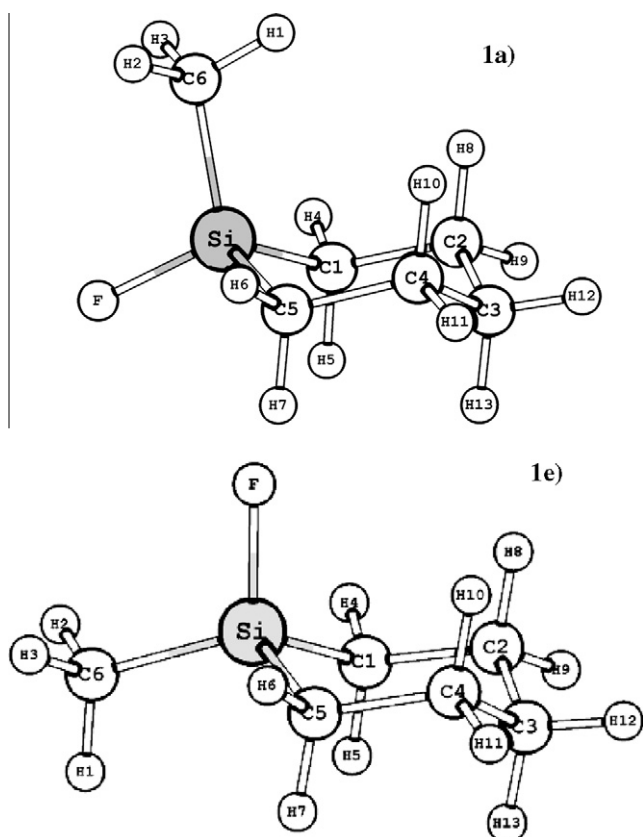


Fig. 1. Structural models of axial **1a** (above) and equatorial **1e** (below) conformers for C<sub>5</sub>H<sub>10</sub>SiFCH<sub>3</sub> with atom numbering.

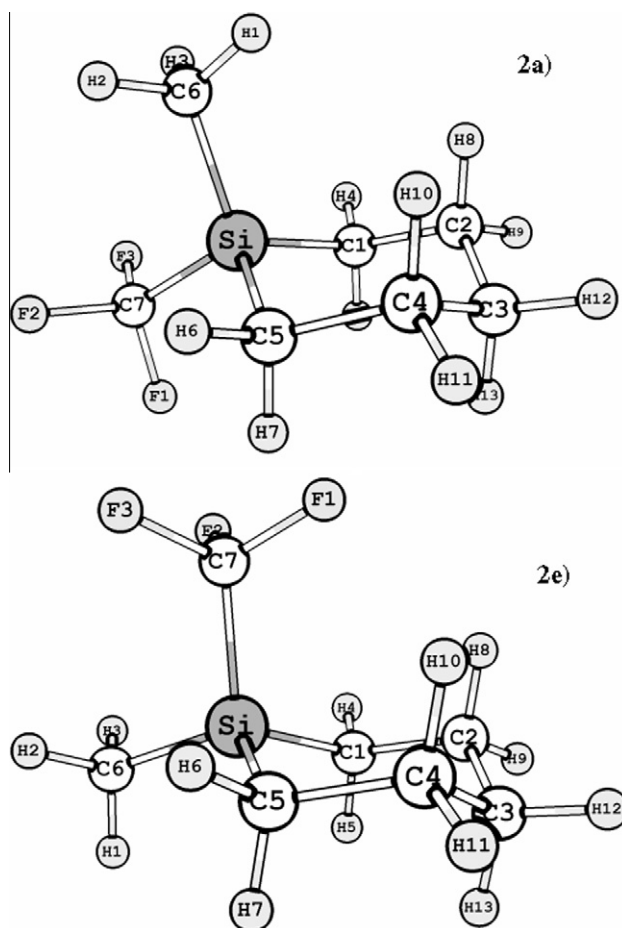


Fig. 2. Structural models of axial **2a** (above) and equatorial **2e** (below) conformers for C<sub>5</sub>H<sub>10</sub>SiC<sub>3</sub>FCH<sub>3</sub> with atom numbering.

coupled cluster calculations, CCSD(T), on M06-2X/pc-2 geometries, were carried out.

The CCSD(T) method, often referred to as the golden standard of quantum chemistry, is an expensive method and usually requires large basis sets for accurate energies.

However, by doing large basis MP2 calculations which are then extrapolated to the complete basis set limit (CBS) and then adding a small basis CCSD(T) correction, accurate CCSD(T)/CBS  $\Delta E$  values can be estimated at affordable cost.

The CCSD(T) correction,  $\delta$ , is usually found to converge rather quickly with increasing basis set [37,38]. The CCSD(T)/CBS estimates are calculated as follows:

$$\Delta E^{\text{CCSD(T)/CBS}} = \Delta E^{\text{MP2/CBS}} + \delta$$

$$\delta = \Delta E^{\text{CCSD(T)/small basis}} - \Delta E^{\text{MP2/small basis}}$$

MP2 calculations were performed with the correlation consistent basis sets [39,40] up to the cc-pV5Z level and were extrapolated to the basis set limit by separate extrapolation of HF energies (T, Q, 5) and MP2 correlation energies (T, Q, 5) by the extrapolation scheme of Helgaker et al. [41]. Details of these calculations are available as supporting information.

The CCSD(T)  $\delta$  correction term was calculated at several different levels to ensure the convergence of the correction, shown in the Supplementary Material (Tables S3 and S4). The calculations suggest the correction to be converged to 0.01–0.02 kcal mol<sup>-1</sup>. The correction calculated with the largest basis set was then added to the MP2/CBS value. This method of extrapolating MP2 energies

and adding a CCSD(T) correction has been used recently to estimate CCSD(T)/CBS  $\Delta E$  values of similar systems [1,42,43].

Thermal corrections to all conformational enthalpies and free energies were done at the B97-1/pc-2 level for consistency; in order to compare quantum chemical conformational energies with the thermodynamical quantities from experiments. B97-1 [44] is known to predict harmonic frequencies and thermal contributions to enthalpy and entropy well [45]. Tight convergence criteria and a large integration grid (int = ultrafine keyword in Gaussian) were used, as the thermal corrections were found to be sensitive to these settings.

In accordance with recent previous work [1,12], the MP2 and CCSD(T) single-point energies are calculated on M06-2X/pc-2 geometries. The M06-2X functional has been found to describe potential energy profiles of small peptides very well [46] (where many functionals fail) where intramolecular dispersion is believed to be important, and its good performance in predicting conformational properties of six-membered rings was the subject of a recent study [12]. We did notice when comparing M06-2X/pc-2 geometries to geometric data from the GED experiments that certain bond lengths of **1** deviated from GED bond lengths more than the B3LYP/6-31G\*\* and MP2/6-31G\*\* values, when predicted by M06-2X/pc-2, although  $r_e$  and  $r_{h1}$  geometries are not necessarily directly compatible. To see how sensitive the single-point energies are on the geometry we carried out CCSD(T) calculations on MP2/cc-pVTZ geometries as well. The difference between  $\Delta E$  values calculated at M06-2X/pc-2 and MP2/cc-pVTZ geometries is less than 0.02 kcal/mol, however. We have thus continued to use M06-2X/pc-2 geometries.

All energies were converged to at least  $1 \times 10^{-6}$  a.u. and geometry optimizations used the default convergence criteria in Gaussian 03 and Gaussian 09. MP2 and CCSD(T) calculations were carried out using the frozen core approximation.

### 3. Results and discussion

#### 3.1. GED analysis

The refinement of the structure and the relative amount of the conformers was carried out by least-squares analyses of the experimental  $sM(s)$  functions. According to quantum chemical calculations two stable conformers of  $C_5H_{10}SiFCH_3$  and  $C_5H_{10}SiCF_3CH_3$  exist (Figs. 1 and 2), axial (**1a**, **2a**) with  $CH_3$  group at axial and equatorial positions (**1e**, **2e**). The theoretical  $sM(s)$  function was constructed under assumption that only two conformers presented in vapour.

Conventional least-squares analyses of  $sM(s)$  were carried out using the modified version of the KCED program [47]. Scattering amplitudes and phases of Ref. [48] were used. The following common assumptions that are based on the quantum chemical calculations (MP2/6-31G\*\*) were made to describe the geometry of the two conformers (atom numbering is given in Figs. 1 and 2) of both  $C_5H_{10}SiFCH_3$  and  $C_5H_{10}SiCF_3CH_3$ : (1) chair conformation of the ring with  $C_s$  overall symmetry, (2) the differences between the C–C bonds as well as the differences between the C–H bonds were constrained to the calculated values, and (3) the  $CH_2$  groups at carbon atoms C2, C3, and C4 were assumed to be oriented symmetrically to the bisector plane of the adjacent endocyclic angle. Calculated deviations from this exact symmetrical orientation (rocking, wagging, and twisting angles) are less than  $1^\circ$ . The rocking angles for the  $CH_2$  groups at carbon atoms C1 and C5, which are larger than  $1^\circ$ , were set to calculated values. The H–C–C bond angles of all  $CH_2$  groups were fixed to the calculated values. (4) The  $CH_3$  group was constrained to  $C_{3v}$  symmetry. The tilt angle was set to zero. Both theoretical methods, MP2/6-31G\*\* and B3LYP/6-31G\*\*, give

values of the tilt angle that are not larger than  $|0.1|^\circ$ . (5) For  $C_5H_{10}SiCF_3CH_3$  the  $CF_3$  group was constrained to  $C_s$  symmetry with equal bond distances C–F and different bond angles F1–C7–F2 and F2–C7–F3.

The refined structural parameters of the axial conformers of  $C_5H_{10}SiFCH_3$  and  $C_5H_{10}SiCF_3CH_3$  molecules are given in Tables 4 and 5, respectively. The independent parameters are marked by symbol  $p_i$ . The 13 independent parameters were used to describe the structure of the **1a** conformer and 16 independent parameters were used for the **2a** conformer. Additionally to these sets the angles Flap(C3) and  $\phi$  (C5–Si1–C1–C2) in the conformers **1e** and **2e** together with the vapour composition were chosen as refined parameters.

The vibrational amplitudes were assembled and refined in groups according to their belonging to the corresponding peaks on the radial distribution curve  $f(r)$ . The differences between vibrational amplitudes within each group were set to the calculated differences. In the least squares fitting of the molecular intensities the geometrical parameters of the equatorial  $CH_3$ -form (excluding the torsional angle around the Si–C1 bond and flap(C3)) were tied to those of the axial- $CH_3$  conformer using the calculated differences. Starting values for bond distances and angles were taken from the MP2/6-31G\*\* calculations, those for vibrational amplitudes as well as the vibrational corrections,  $\Delta r = r_{h1} - r_a$ , for both conformers of  $C_5H_{10}SiFCH_3$  and  $C_5H_{10}SiCF_3CH_3$  molecules were derived from

**Table 4**

Experimental and calculated geometric parameters of axial- $CH_3$  conformer **1a** of  $C_5H_{10}SiFCH_3$  (in Å and deg.). Atom numbering is given in Fig. 1.

	GED $R_f = 3.8\%$ $r_{h1}$ structure	MP2/6-31G** $r_e$ structure	B3LYP/6-31G** $r_e$ structure
Si–C1 $p_1^a$	1.878(4) <sup>f</sup>	1.873	1.881
Si–C6 ( $p_1$ )	1.876(4)	1.872	1.878
C1–C2 $p_2$	1.546(5)	1.541	1.549
C2–C3 ( $p_2$ )	1.538(5)	1.532	1.541
C6–H1 $p_3$	1.094(3)	1.091	1.096
C1–H4 ( $p_3$ )	1.097(3)	1.093	1.097
(C–H) <sub>aver</sub>	1.097(3)	1.093	1.098
Si–F $p_4$	1.630(6)	1.637	1.632
C1–Si–F $p_5$	109.1(8)	110.0	109.4
C1–Si–C5 $p_6$	107.3(5)	104.9	105.1
Si–C1–C2 $p_7$	110.7(3)	110.1	110.9
C1–Si–C6 $p_8$	112.4(5)	112.2	111.9
Si–C6–H1 $p_9$	109.5(14)	110.9	112.2
Tilt ( $CH_3$ ) <sup>b</sup>	0.0 <sup>d</sup>	–0.1	0.1
H1–C6–H2	109.4	107.8	107.7
(H–C–H) <sub>aver</sub> in $CH_2$	106.3 <sup>d</sup>	106.3	106.0
Rock(C1) <sup>c</sup>	2.2 <sup>d</sup>	2.2	2.5
Rock(C2) <sup>c</sup>	0.0 <sup>d</sup>	–0.2	–0.1
Rock(C3) <sup>c</sup>	0.2 <sup>d</sup>	–0.3	–0.4
Flap(C3) $p_{10}$	58.0(37)	57.4	56.3
Flap(Si)	34.9(28)	42.6	40.6
$\phi$ (C5–Si–C1–C2) $p_{11}$	–37.2(28)	–45.7	–43.7
$\phi$ (C1–C2–C3–C4)	–67.7(45)	–65.6	–64.4
$\phi$ (Si–C1–C2–C3)	53.2(16)	56.0	54.5
Flap(C3) $p_{12}^e$	56.2(25)	57.6	56.6
Flap(Si) <sup>e</sup>	34.1(23)	40.8	38.7
$\phi$ (C5–Si–C1–C2) $p_{13}^e$	–36.5(25)	–43.8	–41.7
$\chi$ mol% axial- $CH_3$	45(5)	35	22

Error limits of angles and  $\chi$  are  $2.5\sigma_{LS}$  values. The correlation coefficients had values larger than 0.75:  $p_4/p_2 = -0.96$ ,  $p_5/p_{10} = 0.76$ ,  $p_{12}/p_{10} = 0.96$ .

<sup>a</sup>  $p_i$  – refined parameter; ( $p_i$ ) – the difference with parameter  $p_i$  was set to calculated value.

<sup>b</sup> Tilt( $CH_3$ ) =  $2/3[(Si-C6-H1)-(Si-C6-H2)]$ .

<sup>c</sup> Rock(C1) =  $1/2[(Si-C1-H4)-(Si-C1-H5) + (C2-C1-H4)-(C2-C1-H5)]$ ,

Rock(C2) =  $1/2[(C1-C2-H8)-(C1-C2-H9) + (C3-C2-H8)-(C3-C2-H9)]$ ,

Rock(C3) =  $1/2[(C2-C3-H12)-(C2-C3-H13) + (C4-C3-H12)-(C4-C3-H13)]$ .

<sup>d</sup> Not refined.

<sup>e</sup> Angle in equatorial- $CH_3$  conformer.

<sup>f</sup> Uncertainties for bond lengths  $\sigma = (\sigma_{sc}^2 + (2.5\sigma_{LS})^2)^{1/2}$  ( $\sigma_{sc} = 0.002r$ ,  $\sigma_{LS}$  – standard deviation in least-squares refinement).

**Table 5**

Experimental and calculated geometric parameters of axial-CH<sub>3</sub> conformer **2a** of C<sub>5</sub>H<sub>10</sub>SiCH<sub>3</sub>CF<sub>3</sub> (in Å and deg.). Atom numbering is given in Fig. 2.

	GED $R_f = 4.0\%$	MP2/6-31G**	B3LYP/6-31G**
	$r_{h1}$ structure	$r_e$ structure	$r_e$ structure
Si–C1 $p_1^a$	1.871(4) <sup>f</sup>	1.878	1.889
ΔSiC $p_2$	0.058(22)	0.046	0.045
Si–C7 ( $p_1, p_2$ )	1.929(20)	1.924	1.934
Si–C6 ( $p_1$ )	1.869(4)	1.877	1.884
C1–C2 $p_3$	1.536(3)	1.540	1.548
C2–C3 ( $p_3$ )	1.528(3)	1.533	1.540
C7–F1 $p_4$	1.362(3)	1.366	1.363
C7–F2 ( $p_4$ )	1.362(3)	1.366	1.362
C6–H1 $p_5$	1.088(3)	1.090	1.095
C1–H4 ( $p_5$ )	1.091(3)	1.093	1.096
(C–H) <sub>aver</sub>	1.092(3)	1.094	1.097
C1–Si–C7 $p_6$	108.6(7)	109.0	108.7
C1–Si–C6 $p_7$	114.3(4)	113.3	113.5
C1–Si–C5 $p_8$	108.1(7)	105.3	105.5
Si–C1–C2 $p_9$	111.1(5)	109.9	110.9
Si–C7–F1 $p_{10}$	112.9(5)	112.2	112.2
F1–C7–F2 $p_{11}$	105.6(11)	106.5	106.5
Tilt (CF <sub>3</sub> ) <sup>b</sup>	0.0 <sup>d</sup>	0.1	0.1
Si–C6–H1 $p_{12}^d$	110.9 fix	110.9	111.1
H1–C6–H2	108.1	107.9	107.8
Tilt (CH <sub>3</sub> ) <sup>b,d</sup>	0.	0.	0.
(H–C–H) <sub>aver</sub> in CH <sub>2</sub>	102.6	106.3	106.1
Rock(C1) <sup>c</sup>	2.8	2.8	3.1
Rock(C2) <sup>c</sup>	–0.3	–0.3	–0.4
Rock(C3) <sup>c</sup>	–0.4	–0.4	–0.5
Flap(C3) $p_{13}$	50.9(44)	57.9	56.6
Flap(Si)	33.7(23)	42.1	39.3
φ(C5–Si1–C1–C2) $p_{14}$	–35.9(25)	–44.9	–42.2
φ(C1–C2–C3–C4)	–60.2(49)	–66.2	–65.3
φ(Si–C1–C2–C3)	49.1(15)	55.7	54.0
Flap(C3) $p_{15}^e$	56.2(40)	58.2	57.2
Flap(Si) <sup>e</sup>	28.9(22)	37.8	36.7
φ(C5–Si1–C1–C2) $p_{16}^e$	–31.1(30)	–40.7	–39.6
χ mol% axial-CH <sub>3</sub>	51(5)	38	44

Error limits of angles and χ are 2.5σ<sub>LS</sub> values. The correlation coefficients had values larger than 0.75:  $p_2/p_1 = -0.94$ ,  $p_{10}/p_1 = 0.82$ ,  $p_{10}/p_2 = -0.88$ ,  $p_{11}/p_1 = -0.79$ ,  $p_{11}/p_2 = 0.85$ ,  $p_{11}/p_{10} = -0.96$ ,  $p_{13}/p_{15} = 0.98$ ,  $p_{16}/p_{14} = 0.77$ .

<sup>a</sup>  $p_i$  – refined parameter; ( $p_i$ ) – the difference with parameter  $p_i$  was set to calculated value.

<sup>b</sup> Tilt(CF<sub>3</sub>) = 2/3[(Si–C7–F1)–(Si–C7–F2)].

<sup>c</sup> Rock(C1) = 1/2 [(Si–C1–H4) – (Si–C1–H5) + (C2–C1–H4)–(C2–C1–H5)],

Rock(C2) = 1/2 [(C1–C2–H8) – (C1–C2–H9) + (C3–C2–H8)–(C3–C2–H9)],

Rock(C3) = 1/2 [(C2–C3–H12) – (C2–C3–H13) + (C4–C3–H12) – (C4–C3–H13)].

<sup>d</sup> Not refined.

<sup>e</sup> Angle in equatorial-CH<sub>3</sub> conformer.

<sup>f</sup> Uncertainties for bond lengths  $\sigma = (\sigma_{sc}^2 + (2.5\sigma_{LS})^2)^{1/2}$  ( $\sigma_{sc} = 0.002r$ ,  $\sigma_{LS}$  – standard deviation in least-squares refinement).

calculated (MP2/6-31G\*\*) force fields using the approach of Sipachev incorporated in the program SHRINK [49].

Simultaneous refinement of geometric parameters, vibrational amplitudes, and vapour composition gave the axial-CH<sub>3</sub>:equatorial-CH<sub>3</sub> ratio of 45(6):55(6)% (uncertainty is 2.5σ<sub>LS</sub> value) with  $R_f = 3.8\%$  and 51(5):49(5)% with  $R_f = 4.0\%$  for C<sub>5</sub>H<sub>10</sub>SiFCH<sub>3</sub> and C<sub>5</sub>H<sub>10</sub>SiCF<sub>3</sub>CH<sub>3</sub>, respectively. The correlation coefficients having values larger than 0.75 are given in the footnotes of Tables 4 and 5.

The cross section of the functional  $R_f$  surface along the vapour composition coordinate was studied to check the sensitivity of experimental data to the relative concentration of conformers. The plots of the  $R$  factors vs. percentage of axial-CH<sub>3</sub> conformer **1a** of C<sub>5</sub>H<sub>10</sub>SiFCH<sub>3</sub> and axial-CH<sub>3</sub> conformer **2a** of C<sub>5</sub>H<sub>10</sub>SiCF<sub>3</sub>CH<sub>3</sub> are shown in Fig. 3. The best agreement between experimental and calculated sM(s) functions was achieved at the ratio of axial-CH<sub>3</sub> and equatorial-CH<sub>3</sub> conformers of 45%:55% for C<sub>5</sub>H<sub>10</sub>SiFCH<sub>3</sub> and the ratio of 51%:49% for C<sub>5</sub>H<sub>10</sub>SiCF<sub>3</sub>CH<sub>3</sub>, respectively. The uncertainty in the vapour composition was estimated by Hamilton's method [50] and was found to be about 15% at the significance level of 0.05 (see Fig. 3).

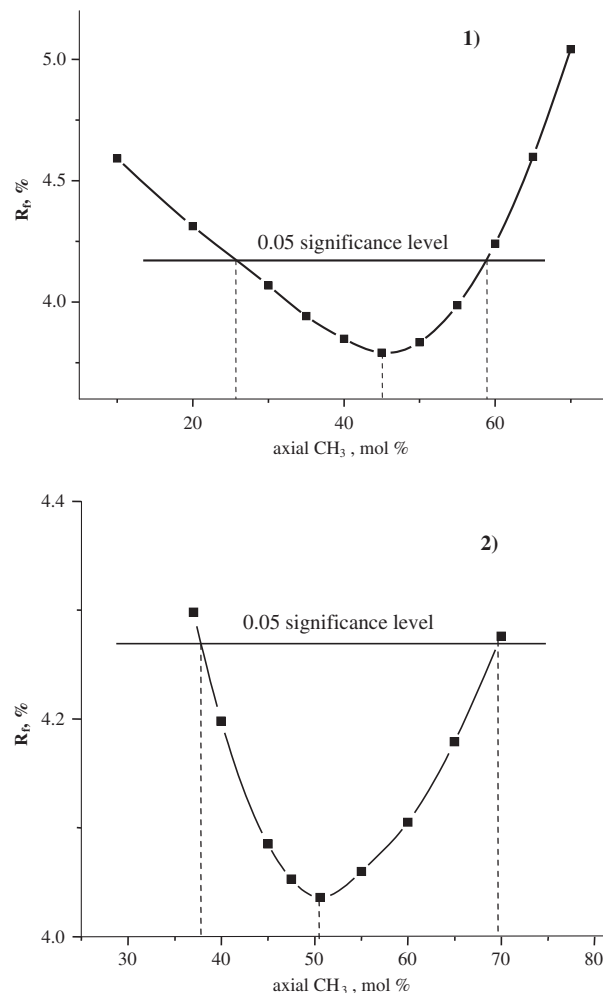


**Fig. 3.** Agreement factor  $R_f$  for different contributions of axial conformer: (1) for C<sub>5</sub>H<sub>10</sub>SiFCH<sub>3</sub> and (2) for C<sub>5</sub>H<sub>10</sub>SiCF<sub>3</sub>CH<sub>3</sub>.

The experimental structural parameters for the axial-CH<sub>3</sub> conformers **1a** and **2a** together with calculated values are listed in Tables 4 and 5 for C<sub>5</sub>H<sub>10</sub>SiFCH<sub>3</sub> and C<sub>5</sub>H<sub>10</sub>SiCF<sub>3</sub>CH<sub>3</sub>, respectively. In addition to the refined independent parameters some important dependent parameters are also shown in the tables. Interatomic distances, experimental and calculated vibrational amplitudes and vibrational corrections (without non-bonded distances involving hydrogen atoms) are listed in the Supplementary Material (Tables S1 and S2) for C<sub>5</sub>H<sub>10</sub>SiFCH<sub>3</sub> and C<sub>5</sub>H<sub>10</sub>SiCF<sub>3</sub>CH<sub>3</sub>, respectively.

Two radial distribution functions  $f(r)$  reserved with fixed vapour composition at 100% axial or 100% equatorial conformers and corresponded to the refined other independent parameters are shown in Fig. 4. For both molecules both functions differ appreciably in the range  $r > 3.6$  Å, which contains the peaks corresponding to long non-bonded distances between the substituent groups at Si atoms and the atoms C and H of the six-membered ring. This difference demonstrates that the electron diffraction intensities are sensitive towards the conformational properties of these compounds. Comparison with the experimental radial distribution function  $f(r)$ , which was derived by Fourier transformation of the molecular intensities sM(s), demonstrates that both conformers are present in the vapour of C<sub>5</sub>H<sub>10</sub>SiFCH<sub>3</sub> and C<sub>5</sub>H<sub>10</sub>SiCF<sub>3</sub>CH<sub>3</sub> under the conditions of the GED experiment in approximately equal concentrations.

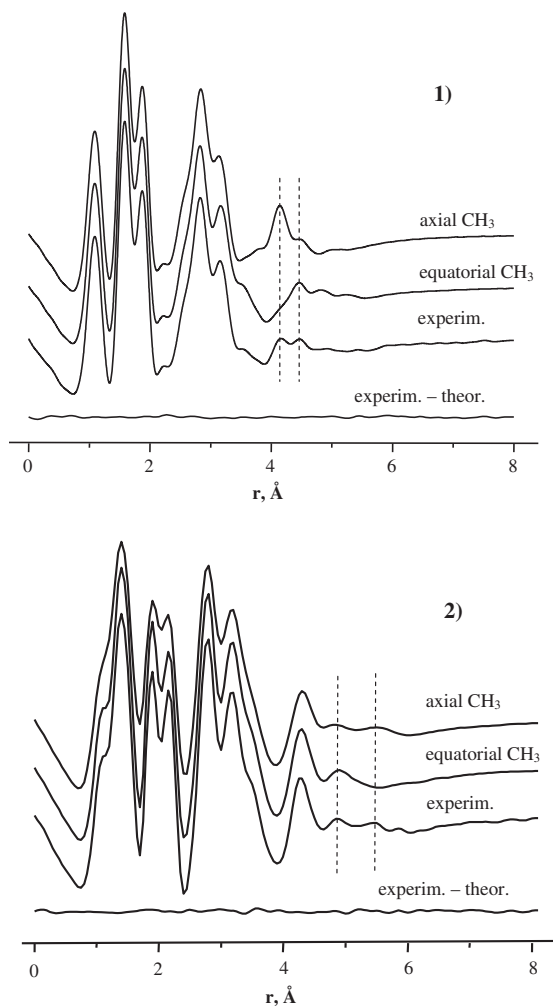


**Fig. 4.** Radial distribution functions for refined geometries of axial conformer (100% in the vapour assumed) and equatorial conformer (100% in the vapour assumed), and experimental function and difference curve for mixture (vapour composition was refined): (1) for  $C_5H_{10}SiFCH_3$  and (2) for  $C_5H_{10}SiCH_3CF_3$ .

### 3.2. NMR spectroscopy

The  $^{19}F$  NMR spectra of both compounds at room temperature show rapid interconversion of the axial and equatorial conformers. On cooling in the region 180–115 K, the spectra (Fig. 5) show line broadening and gradual splitting of the  $^{19}F$  NMR signal into two components indicating a mixture of two conformers, with coalescence points near 149 and 124 K for compounds **1** and **2**, respectively. Calculations for **1** and 1-fluoro-1-silacyclohexane predict the resonance signals for  $^{19}F$  in the axial position to appear at lower  $\delta$  (higher field) than the signal for the same substituent in the equatorial position (see Table 6 and Ref. [10]). The opposite is found for the  $^{19}F$  resonance signal of compound **2** and 1-trifluoromethyl-1-silacyclohexane, i.e. calculations predict the resonance signal for  $^{19}F$  in  $CF_3$  in the axial position to appear at higher  $\delta$  (lower field) than the signal for the same substituent in the equatorial position (see Table 6 and Refs. [8,9]). Hence, based on the relative peak intensities (Fig. 5), the conformation with the fluorine containing substituent in axial position is found to be in excess for both compounds, **1** and **2**.

Dynamic NMR simulations of the spectra, by using the software WinDNMR [23] as shown in Fig. 5 allowed determination of the rate constants ( $k_{e \rightarrow a}$ ) and the corresponding free energies of activation ( $\Delta G_{e \rightarrow a}^\ddagger$ ) as a function of temperature. Chemical shifts,

derived from NMR spectra which were recorded for the lowest temperatures, were assumed to represent conditions of negligible interconversions (see Table 7). The derived rate constants indicate slightly increasing  $\Delta G_{e \rightarrow a}^\ddagger$  values with temperature for both compounds. Average values for  $\Delta G_{e \rightarrow a}^\ddagger$  are listed in Table 7. Furthermore, the equilibrium constants ( $K_{e \rightarrow a}$ ) (hence free energy changes,  $\Delta G_{e \rightarrow a}$ ) for the equatorial to axial transformations, corresponding to temperatures slightly below the coalescence points ( $\Delta T \sim 123$ – $132$  K for **1** and  $\Delta T \sim 113$ – $122$  K for **2**) could be determined from the relative signal intensities. More information on the DNMR analysis is given as Supplementary Material.

### 3.3. Raman spectroscopy

We have in previous publications used temperature-dependent Raman spectroscopy to analyse the ratio of axial and equatorial conformers in monosubstituted silacyclohexanes [1,10]. The application of the method to this problem has been described in detail in one of the publications [1], therefore only a brief description will be given here. Temperature-dependent Raman spectra of compounds are typically analysed using the van't Hoff relation  $\ln(A_1/A_2) = -\Delta H/RT + \text{constant}$ , where  $A_1$  and  $A_2$  are the intensities of the vibrational bands belonging to two different conformers of the molecule. Either the heights or areas of the bands can be used for the  $A_1/A_2$  ratio. The relation is correct under the assumption that  $\Delta H$  and the Raman scattering coefficients are temperature independent.

Low-temperature spectra were recorded for pure **1** and **2** at temperatures varying from 300 to 210 K, at 15 K intervals. Spectra were also recorded for the two compounds in THF solution (300–210 K, 15 K intervals) and hexane solution (300–210 K, 15 K intervals). The Raman spectrum of pure **1** at room temperature in the range 150–1450  $cm^{-1}$  can be seen in Fig. 6. Fig. 6 also includes an expansion of the 575–635  $cm^{-1}$  range, where the symmetrical  $SiC_2$  vibrations ( $\nu_s SiC_2$ ) occur. The calculated wavenumbers (based on quantum chemical frequency calculations using the B3LYP/6-31G(d,p) method) for these vibration are: 585  $cm^{-1}$  for conformer **1a** and 597  $cm^{-1}$  for conformer **1e**. The calculated values enabled the assignment of the experimental values of 607 and 614  $cm^{-1}$  as belonging to conformers **1a** and **1e**, respectively. Although this wavenumber difference is rather small, it was sufficient to give distinguished signals for both conformers, albeit slightly overlapping ones. As the intensities of the bands varied with temperature, van't Hoff analysis was deemed appropriate. Fig. 7 shows the Raman spectrum of pure **2** at room temperature in the range 150–1500  $cm^{-1}$  along with an expansion of the 570–675  $cm^{-1}$  range where the symmetrical  $SiC_2$  vibrations ( $\nu_s SiC_2$ ) occur. The calculated vibrational values of these vibrations were found to be 598  $cm^{-1}$  (**2a**) and 617  $cm^{-1}$  (**2e**), while the experimental values were measured as 619 and 629  $cm^{-1}$ , respectively. Again the intensities varied with temperature.

Fig. 8 shows the van't Hoff plots of pure liquid **1** using both peak heights and peak areas. The analysis is based on the temperature dependent  $A_1/A_2$  ratio of the  $\nu_s SiC_2$  vibrational bands. The calculated enthalpy differences from the van't Hoff analysis were found to be:  $\Delta H_{e \rightarrow a, \text{heights}} = 0.50$  kcal mol $^{-1}$  using peak heights and  $\Delta H_{e \rightarrow a, \text{areas}} = 0.61$  kcal mol $^{-1}$  using peak areas ( $\Delta H_{e \rightarrow a} = H_{ax} - H_{eq}$ ). Fig. 9 shows analogous results for pure **2**, where the calculated enthalpy differences were found to be:  $\Delta H_{e \rightarrow a, \text{heights}} = 0.73$  kcal mol $^{-1}$  and  $\Delta H_{e \rightarrow a, \text{areas}} = 0.60$  kcal mol $^{-1}$ .

The results from the analysis of low-temperature Raman measurements are shown in Tables 8 and 9 for **1** and **2**, respectively, along with energetic results from GED and DNMR experiments as well as QC calculations. From the tables it can be deduced that the different polarities of the media do not influence the  $\Delta H$  values as they remain fairly constant, within an error limit of  $\pm 0.1$  kcal -

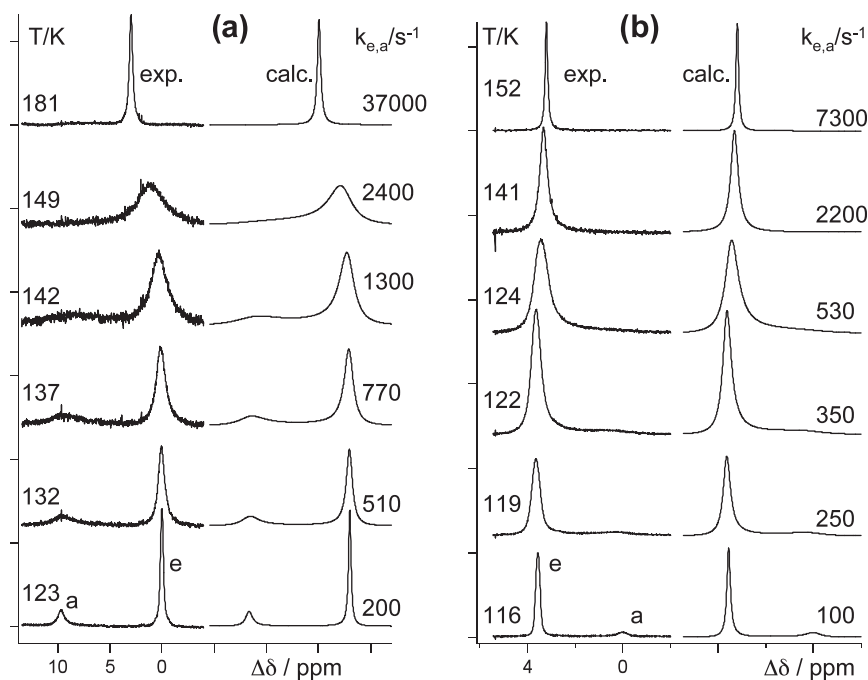


**Fig. 5.** Simulations of the  $^{19}\text{F}$  NMR spectra for (a) **1** and (b) **2** in a 1:1:3 mixture of  $\text{CD}_2\text{Cl}_2$ ,  $\text{CHFCl}_2$ , and  $\text{CHF}_2\text{Cl}$  as a function of temperature. Experimental spectra are on the left and calculated spectra on the right.

**Table 6**

PBE1PBE/aug-pcS-2 calculated  $^{19}\text{F}$  chemical shifts (relative to  $\text{CFCl}_3$ ) of the axial and equatorial conformers of **1** and **2** (in ppm) compared to experimental chemical shifts (in ppm) from DNMR experiments.

Method	Atoms	Axial	Equatorial	Difference (e–a)
<b>1</b>				
GIAO-PBE1PBE	F	–186.7	–198.4	–11.7
Experiment	F	–163.0	–172.7	–9.7
<b>2</b>				
GIAO-PBE1PBE	$^{19}\text{F} + ^{21}\text{F}$	–83.0	–80.9	2.1
	$^{20}\text{F}$	–83.7	–72.6	11.1
	Mean (F)	–83.3	–76.8	6.5
Experiment	F	–65.7	–62.1	3.6

**Table 7**

Parameters relevant to conformational equilibria and rates of exchanges derived from dynamic NMR simulations of  $^{19}\text{F}$ -NMR spectra.

Parameters	Compound	
	<b>1</b>	<b>2</b>
Coalescence point temperature, K	149(5)	124(5)
$\Delta G_{e \rightarrow a}^\ddagger$ (kcal mol $^{-1}$ )	6.2(1)	5.6(2)
%a:%e	26:74/125 K <sup>a</sup>	16:84/118 K <sup>b</sup>
$K_{e \rightarrow a}$	0.35(4)/125 K <sup>a</sup>	0.19(4)/118 K <sup>b</sup>
$\Delta G_{e \rightarrow a}$ (kcal mol $^{-1}$ )	0.26(3)/125 K <sup>a</sup>	0.39(3)/118 K <sup>b</sup>

<sup>a</sup> Average values in the temperature range 123–132 K.

<sup>b</sup> Average values in the temperature range 113–122 K.

mol $^{-1}$  proposed in previous work [1]. The  $\Delta H$  values are more affected by the choice of how the  $A_1/A_2$  ratio is measured. On average there is a 0.1 kcal mol $^{-1}$  difference between the  $\Delta H$  values derived from the peak heights and from the peak areas. Peak areas are notoriously inaccurate for overlapping peaks, as they have to be determined by a more difficult method of deconvolution than used for peak heights, therefore we use the results from peak heights only in Tables 8 and 9. We have, however, increased the range of uncertainty to  $\pm 0.15$  kcal mol $^{-1}$ . More information on the Raman experiments is available as Supporting Material Figs. S2–S7).

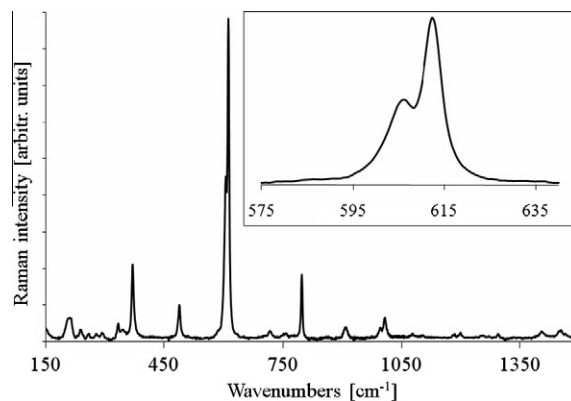


**Fig. 6.** Raman spectrum of pure liquid **1** at room temperature. The range 575–635  $\text{cm}^{-1}$ , which includes the conformation-sensitive symmetrical  $\text{SiC}_2$  vibrations, has been expanded for illustrative purposes.

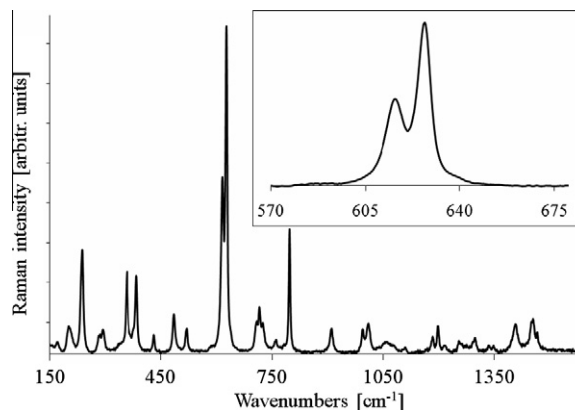


**Fig. 7.** Raman spectrum of pure liquid **2** at room temperature. The range 570–675  $\text{cm}^{-1}$ , which includes the conformation-sensitive symmetrical  $\text{SiC}_2$  vibrations, has been expanded for illustrative purposes.

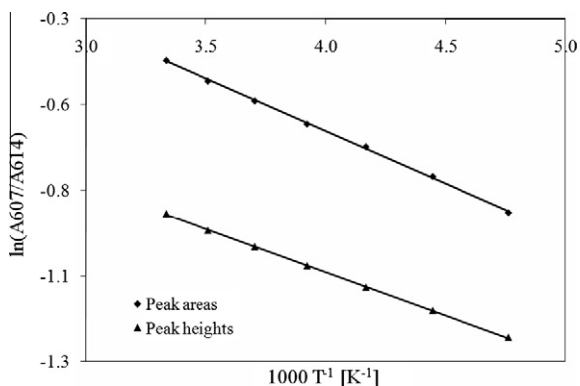


**Fig. 8.** van't Hoff plot of the band pair 607/614  $\text{cm}^{-1}$  of pure **1** using peak areas (diamonds) and peak heights (triangles).

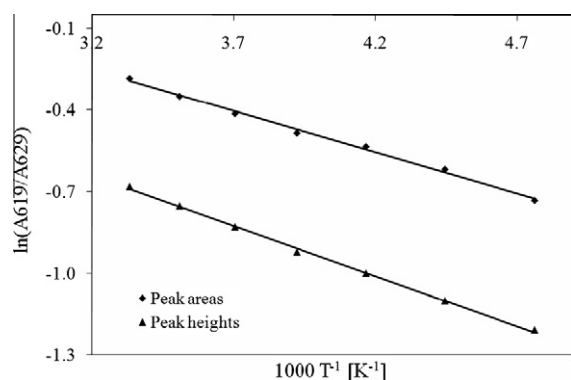


**Fig. 9.** Van't Hoff plot of the band pair 619/629  $\text{cm}^{-1}$  of pure **2** using peak areas (diamonds) and peak heights (triangles).

**Table 8**  
Conformational properties of  $\text{C}_5\text{H}_{10}\text{SiFCH}_3$  (**1**).

Calculations	$T = 0 \text{ K}$ $\Delta E = E_{\text{ax}} - E_{\text{eq}}$ (kcal mol $^{-1}$ )	$T = 300\text{--}210 \text{ K}$ $\Delta H = H_{\text{ax}} - H_{\text{eq}}$ (kcal mol $^{-1}$ )	$T = 125 \text{ K}$ $A = G_{\text{ax}} - G_{\text{eq}}$ (kcal mol $^{-1}$ )	$T = 282 \text{ K}$ $A = G_{\text{ax}} - G_{\text{eq}}$ (kcal mol $^{-1}$ )
CCSD(T)/CBS <sup>a</sup>	0.23			
CCSD(T)/CBS <sup>a</sup> + therm. corr. <sup>b</sup>		0.25	0.28	0.31
Experiment				
GED				0.11(13)
Raman, neat		0.50(15)		
Raman, in THF		0.51(15)		
Raman, in hexane		0.48(15)		
NMR			0.26(2)	

<sup>a</sup> The CCSD(T)/CBS electronic energies are single-point energies at M06-2X/pc-2 geometries and are zero-point energy exclusive.

<sup>b</sup> The thermal correction term (consisting of zero-point energy, enthalpic and entropic corrections at the indicated temperatures) is calculated at the B97-1/pc-2 level for all cases.

### 3.4. Computational studies

The minimum energy pathways of ring inversion of both molecules were calculated and are shown in Figs. 10 and 11. The inversion path from the axial conformer to the equatorial conformer consists of a half-chair/sofa like transition state from where the molecule moves into a twist form of rather high energy. The molecule then goes through a boat form to a more stable twist form at the midpoint of the path. Going through a second boat transition state, another twist minimum and a half-chair/sofa transition state, the molecule finally ends up in the equatorial form.

**Table 9**  
Conformational properties of  $\text{C}_5\text{H}_{10}\text{CH}_2\text{CF}_3$  (**2**).

Calculations	$T = 0 \text{ K}$ $\Delta E = E_{\text{ax}} - E_{\text{eq}}$ (kcal mol $^{-1}$ )	$T = 300\text{--}210 \text{ K}$ $\Delta H = H_{\text{ax}} - H_{\text{eq}}$ (kcal mol $^{-1}$ )	$T = 118 \text{ K}$ $A = G_{\text{ax}} - G_{\text{eq}}$ (kcal mol $^{-1}$ )	$T = 262 \text{ K}$ $A = G_{\text{ax}} - G_{\text{eq}}$ (kcal mol $^{-1}$ )
CCSD(T)/CBS <sup>a</sup>	0.49			
CCSD(T)/CBS <sup>a</sup> + therm. corr. <sup>b</sup>		0.48	0.36	0.22
Experiment				
GED				-0.02(11)
Raman, neat		0.73(15)		
Raman, in THF		0.78(15)		
Raman, in hexane		0.67(15)		
NMR			0.39(2)	

<sup>a</sup> The CCSD(T)/CBS electronic energies are single-point energies at M06-2X/pc-2 geometries and are zero-point energy exclusive.

<sup>b</sup> The thermal correction term (consisting of zero-point energy, enthalpic and entropic corrections at the indicated temperatures) is calculated at the B97-1/pc-2 level for all cases.

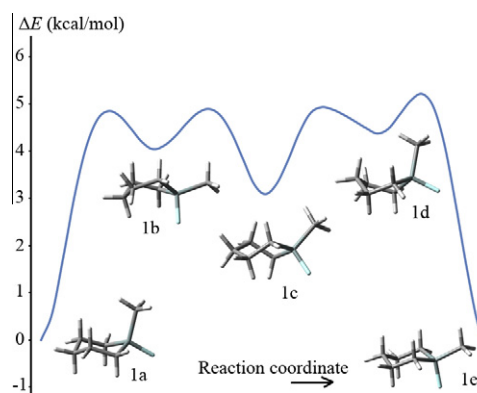


**Fig. 10.** M06-2X/pc-2 minimum energy pathway for the chair-to-chair inversion of  $\text{C}_5\text{H}_{10}\text{SiFCH}_3$  (**1**). 1a and 1e correspond to the axial and equatorial conformers, respectively. 1b–1d correspond to three different twist forms.

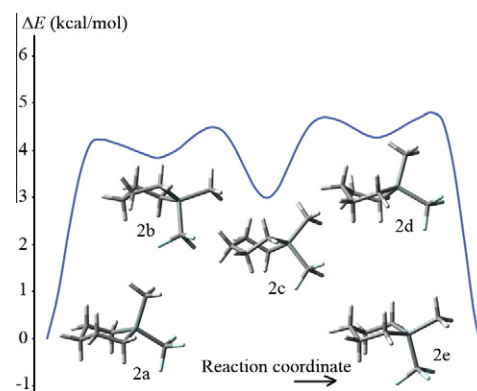


**Fig. 11.** M06-2X/pc-2 minimum energy pathway for the chair-to-chair inversion of  $\text{C}_5\text{H}_{10}\text{SiCH}_2\text{CF}_3$  (**2**). 2a and 2e correspond to the axial and equatorial conformers, respectively. 2b–2d correspond to three different twist forms.

Elaborate CCSD(T)/CBS conformational energy differences of both molecules with B97-1/pc-2 thermal corrections are compared with the experimental conformational energy differences in Tables 8 and 9.

It should be pointed out, however, that our B97-1/pc-2 corrections are based on the harmonic oscillator approximation. Six-membered rings include a number of low-frequency vibrations that are known to be badly predicted by the harmonic approxima-

tion. As these vibrations contribute significantly to entropy, errors in the free energy correction can be expected. This problem has been noted recently in the literature for another ring system, cyclooctane [51], and for substituted ethanes [52] where the failure of the harmonic approximation to properly describe low-frequency vibrations was found to greatly affect the thermal contribution to entropy and hence the free energy difference of conformers. Unfortunately, a solid method to account for low-frequency vibrations of systems such as ours, does not exist and we are therefore relying on cancellation of errors.

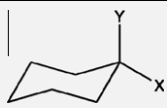
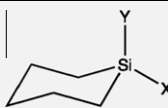
We made no attempt to model the possible contribution of the solvent on the enthalpy and free energy differences of the Raman and NMR experiments. The Raman experiments suggest solvents of different polarity to have a very small effect on the axial/equatorial energy difference and we have previously met with little success in accounting for solvent effects with continuum solvation models [1,8,9].

From the results in Tables 8 and 9, we note that it is not the gas electron diffraction  $\Delta G$  values (which should be free from intermolecular effects) that is in best agreement with the calculated  $\Delta G$  results but rather the  $\Delta G$  value from the NMR experiment. This has been noticed before [1]. For molecule 1, the B97-1/pc-2 thermal correction (at GED experimental temperatures) increases deviation with experiment (compared to the uncorrected  $\Delta E$  value), predicting further stabilization for the conformer 1e, while for 2 the deviation decreases. We believe the deviation between calculated  $\Delta G$  values and GED  $\Delta G$  values may result from assumed harmonicity of low-frequency modes in the B97-1/pc-2 thermal correction.

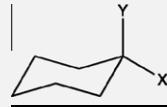
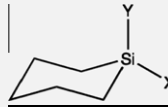
The low-temperature NMR experimental  $\Delta G$  values, on the other hand, are in much better agreement with the calculated  $\Delta G$  values (and even the  $\Delta E$  values). The B97-1/pc-2 thermal free energy corrections are here predicted to be smaller at the NMR temperatures (124 and 149 K) compared to the corrections at the GED experimental temperatures (282 and 262 K).

Presumably, as the entropy term of the free energy is temperature-dependent, the free energy difference approaches the enthalpy difference (and approximately the electronic energy difference) in the low-temperature NMR experiment.

**Table 10**  
Comparison of the conformational properties of mono- and disubstituted cyclohexane and silacyclohexane. CCSD(T)/CBS calculated  $\Delta E(E_{ax}-E_{eq})$  values in kcal mol<sup>-1</sup>.

Substituent X/Y		
F/H	0.15	-0.15
CH <sub>3</sub> /H	1.75	0.17
CF <sub>3</sub> /H	2.28	-0.44
CH <sub>3</sub> /F	0.86	0.23
CH <sub>3</sub> /CF <sub>3</sub>	-1.31	0.49

**Table 11**  
Additivity of substituents in disubstituted cyclohexanes and silacyclohexanes. CCSD(T)/CBS values calculated  $\Delta E(E_{ax}-E_{eq})$  values in kcal mol<sup>-1</sup> taken from Table 10.

						
	Monosub. added <sup>a</sup>	Disub. calc. <sup>b</sup>	Difference	Monosub. added <sup>a</sup>	Disub. calc. <sup>b</sup>	Difference
CH <sub>3</sub> (eq) + F(ax)	1.60	0.86	0.74	0.32	0.23	0.09
CH <sub>3</sub> (eq) + CF <sub>3</sub> (ax)	-0.53	-1.31	0.78	0.61	0.49	0.12

<sup>a</sup> Assumed additivity of substituent effects.

<sup>b</sup> Calculated value for disubstituted ring.

The Raman  $\Delta H$  value is for both molecules rather larger in magnitude than the calculated  $\Delta H$  value and the  $\Delta G$  values from GED and NMR experiments. This deviation cannot easily be explained. A systematic error in the Raman measurements cannot be ruled out. A moderate disagreement between Raman measurements and calculations was also noticed for silylsilacyclohexane [1].

#### 4. Conclusions

To conclude, while a perfect agreement between theory and experiment was not reached, the deviations seem to be due to thermal effects at different experimental conditions that are not easy to account for; furthermore these effects are unrelated to the potential energy part of the conformational energy surface, which is what distinguishes silacyclohexanes from cyclohexanes in the first place.

Finally, in order to offer an answer to the proposed question in the introduction about additive conformational  $A$  values of silacyclohexanes, we decided to focus our attention on the potential energy (and not thermal effects) and thus carried out similar CCSD(T)/CBS calculations (on M06-2X/pc-2 geometries) of both monosubstituted silacyclohexanes with substituents F, CH<sub>3</sub>, and CF<sub>3</sub> and mono- and disubstituted cyclohexanes with the same substituents. The results of these calculations are shown in Table 10. These results can then be used further to estimate how well the  $\Delta E$  values for the two ring systems are additive in respect of individual substituents. In doing so, one has to bear in mind that in monosubstituted six-membered rings the hydrogen atom also acts as a substituent and it may influence the conformational equilibrium differently in the axial and equatorial position, respectively. We will neglect the possible substituent effect by the H atom. In Table 11 the addition of the substituent effects of two substituents, one in the equatorial and the other in the axial position is compared to the calculated values for the equally disubstituted rings. The addition model works only moderately well for the cyclohexanes, the fact that the difference is virtually the same in both cases is most likely a coincidence. For the silacyclohexanes, however, the model works remarkably well for this limited selection of substituents. Further studies will reveal if the addition model is a general effect for silicon-containing six-membered rings.

#### Acknowledgements

A financial support from 'The Icelandic Research Fund' (Grant No. 080038021) is gratefully acknowledged. Use of the computing resources of the University of Iceland Computer Services and the EaStCHEM Research Computing facility are acknowledged. G.V.G. and N.I.G. are grateful to the RFBR (Grant 09-03-91341\_NNIOa) for financial support. K.H. thanks the 'Fonds zur Förderung der wissenschaftlichen Forschung' (FWF), Vienna, for financial support of project P 18176-N11. The authors are grateful to Mr. D. Müller at

the University Karlsruhe for carrying out HRMS of the title compounds.

### Appendix A. Supplementary data

Following material is available for both title compounds. Molecular intensity curves. Tables of interatomic distances, experimental and calculated vibrational amplitudes and vibrational corrections. Simulated spectra and parameters derived from the DNMR analysis. Time-dependent Raman spectra of pure compounds. van't Hoff plots in hexane and THF solution. The convergence of the  $\delta$  correction used in the  $\Delta E$  CCSD(T)/CBS estimate. Total energies and relative energies of the minimum energy pathway for the chair-to-chair inversion. M06-2X/pc-2 molecular geometries for the chair conformers. Tables of total and relative energies. Shielding constants and relative chemical shifts for the fluorine nuclei at M06-2X/pc-2 geometries. Supplementary data associated with this article can be found, in the online version, at doi:10.1016/j.molstruc.2010.02.059.

### References

- [1] S.Ó. Wallevik, R. Björnsson, Á. Kvaran, S. Jonsdóttir, I. Arnason, A.V. Belyakov, A.A. Baskakov, K. Hassler, H. Oberhammer, *J. Phys. Chem. A* 114 (2010) 2127.
- [2] C.H. Bushweller. In: E. Juaristi (Ed.), *Conformational Behavior of Six-Membered Rings*, VCH Publishers, Inc., New York, 1995, p. 25.
- [3] E.L. Eliel, S.H. Wilen, *Stereochemistry of Organic Compounds*, Wiley, New York, 1994.
- [4] S. Winstein, N.J. Holness, *J. Am. Chem. Soc.* 77 (1955) 5562.
- [5] I. Arnason, Á. Kvaran, A. Bodi, *Int. J. Quantum Chem.* 106 (2006) 1975.
- [6] I. Arnason, G.K. Thorarinnsson, E. Matern, *Z. Anorg. Allg. Chem.* 626 (2000) 853.
- [7] I. Arnason, A. Kvaran, S. Jonsdóttir, P.I. Gudnason, H. Oberhammer, *J. Org. Chem.* 67 (2002) 3827.
- [8] G.V. Girichev, N.I. Giricheva, A. Bodi, P.I. Gudnason, S. Jonsdóttir, A. Kvaran, I. Arnason, H. Oberhammer, *Chem. Eur. J.* 13 (2007) 1776.
- [9] G.V. Girichev, N.I. Giricheva, A. Bodi, P.I. Gudnason, S. Jonsdóttir, A. Kvaran, I. Arnason, H. Oberhammer, *Chem. Eur. J.* 15 (2009) 8929.
- [10] A. Bodi, Á. Kvaran, S. Jonsdóttir, E. Antonsson, S.Ó. Wallevik, I. Arnason, A.V. Belyakov, A.A. Baskakov, M. Hölbling, H. Oberhammer, *Organometallics* 26 (2007) 6544.
- [11] S.O. Wallevik, M.Sc. Thesis, University of Iceland, 2008.
- [12] R. Björnsson, I. Arnason, *Phys. Chem. Chem. Phys.* 11 (2009) 8689.
- [13] A. Tsuboyama, A. Murayama, S. Konaka, M. Kimura, *J. Mol. Struct.* 118 (1984) 351.
- [14] P. Andersen, *Acta Chem. Scand.* 16 (1962) 2337.
- [15] Y. Carcenac, P. Diter, C. Wakselman, M. Tordeux, *New. J. Chem.* 30 (2006) 442.
- [16] C. Zheng, S. Subramaniam, V.F. Kalasinsky, J.R. Durig, *J. Mol. Struct.* 785 (2006) 143.
- [17] E.L. Eliel, R.M. Enanoza, *J. Am. Chem. Soc.* 94 (1972) 8072.
- [18] D.J. Hodgson, U. Rychlewska, E.L. Eliel, M. Manoharan, D.E. Knox, E.M. Olefirowicz, *J. Org. Chem.* 50 (1985) 4838.
- [19] R. West, *J. Am. Chem. Soc.* 76 (1954) 6012.
- [20] G.V. Girichev, S.A. Shlykov, Y.F. Revichev, *Prib. Tekh. Eksp. N4* (1986) 167; (in Russian); *Instrum. Exp. Tech. (English Transl.)* 2 (1984) 457, 4 (1986) 167.
- [21] G.V. Girichev, A.N. Utkin, Y.F. Revichev, *Prib. Tekh. Eksp. N2* (1984) 187 (in Russian); *Instrum. Exp. Tech. (English Transl.)* 2 (1984) 457, N2 (1984) 187.
- [22] E.G. Girichev, A.V. Zakharov, G.V. Girichev, M.I. Bazanov, *Izv. VUZ Tekstiln. Prom.* 2 (2000) 142 (in Russian).
- [23] H.J. Reich, WinDNMR: Dynamic NMR Spectra for Windows, *J. Chem. Educ. Software 3D2*. Available from: <[http://jchemed.chem.wisc.edu/JCESoft/Issues/Series\\_D/3D2/prog1-3D2.html](http://jchemed.chem.wisc.edu/JCESoft/Issues/Series_D/3D2/prog1-3D2.html)>.
- [24] M.J. Frisch, G.W. Trucks, H.B. Schlegel, G.E. Scuseria, M.A. Robb, J.R. Cheeseman, J.J.A. Montgomery, T. Vreven, K.N. Kudin, J.C. Burant, J.M. Millam, S.S. Iyengar, J. Tomasi, V. Barone, B. Mennucci, M. Cossi, G. Scalmani, N. Rega, G.A. Petersson, H. Nakatsuji, M. Hada, M. Ehara, K. Toyota, R. Fukuda, J. Hasegawa, M. Ishida, T. Nakajima, Y. Honda, O. Kitao, H. Nakai, M. Klene, X. Li, J.E. Knox, H.P. Hratchian, J.B. Cross, V. Bakken, C. Adamo, J. Jaramillo, R. Gomperts, R.E. Stratmann, O. Yazyev, A.J. Austin, R. Cammi, C. Pomelli, J.W. Ochterski, P.Y. Ayala, K. Morokuma, G.A. Voth, P. Salvador, J.J. Dannenberg, V.G. Zakrzewski, S. Dapprich, A.D. Daniels, M.C. Strain, O. Farkas, D.K. Malick, A.D. Rabuck, K. Raghavachari, J.B. Foresman, J.V. Ortiz, Q. Cui, A.G. Baboul, S. Clifford, J. Cioslowski, B.B. Stefanov, G. Liu, A. Liashenko, P. Piskorz, I. Komaromi, R.L. Martin, D.J. Fox, T. Keith, M.A. Al-Laham, C.Y. Peng, A. Nanayakkara, M. Challacombe, P.M.W. Gill, B. Johnson, W. Chen, M.W. Wong, C. Gonzalez, J.A. Pople, *Gaussian 03, Revision C.02*, Wallingford, CT, 2004.
- [25] M.J. Frisch, G.W. Trucks, H.B. Schlegel, G.E. Scuseria, M.A. Robb, J.R. Cheeseman, G. Scalmani, V. Barone, B. Mennucci, G.A. Petersson, H. Nakatsuji, M. Caricato, X. Li, H.P. Hratchian, A.F. Izmaylov, J. Bloino, G. Zheng, J.L. Sonnenberg, M. Hada, M. Ehara, K. Toyota, R. Fukuda, J. Hasegawa, M. Ishida, T. Nakajima, Y. Honda, O. Kitao, H. Nakai, T. Vreven, J.A. Montgomery Jr., J.E. Peralta, F. Ogliaro, M. Bearpark, J.J. Heyd, E. Brothers, K.N. Kudin, V.N. Staroverov, R. Kobayashi, J. Normand, K. Raghavachari, A. Rendell, J.C. Burant, S.S. Iyengar, J. Tomasi, M. Cossi, N. Rega, J.M. Millam, M. Klene, J.E. Knox, J.B. Cross, V. Bakken, C. Adamo, J. Jaramillo, R.E. Gomperts, O. Stratmann, A.J. Yazyev, R. Austin, C. Cammi, J.W. Pomelli, R. Ochterski, R.L. Martin, K. Morokuma, V.G. Zakrzewski, G.A. Voth, P. Salvador, J.J. Dannenberg, S. Dapprich, A.D. Daniels, O. Farkas, J.B. Foresman, J.V. Ortiz, J. Cioslowski, D. Fox, *Gaussian 09, Revision A.02*, Wallingford, CT, 2009.
- [26] H.-J. Werner, P.J. Knowles, R. Lindh, F.R. Manby, M. Schütz, P. Celani, T. Korona, G. Rauhut, R.D. Amos, A. Bernhardsson, A. Berning, D.L. Cooper, M.J.O. Deegan, A.J. Dobbyn, F. Eckert, A.W.L.C. Hampel, G. Hetzer, S.J. McNicholas, W. Meyer, M.E. Mura, A. Nicklass, P. Palmieri, R. Pitzer, U. Schumann, H. Stoll, A.J. Stone, R. Tarroni, T. Thorsteinsson, *MOLPRO, version 2006.1*, a package of ab initio programs, 2006, see <<http://www.molpro.net/>>.
- [27] R. Dichtfield, *Mol. Phys.* 27 (1974) 789.
- [28] K. Wolinski, J.F. Hinton, P.J. Pulay, *J. Am. Chem. Soc.* 112 (1990) 8251.
- [29] C. Adamo, V. Barone, *J. Chem. Phys.* 110 (1999) 6158.
- [30] C. Adamo, V. Barone, *Chem. Phys. Lett.* 298 (1998) 113.
- [31] F. Jensen, *J. Chem. Theory. Comput.* 4 (2008) 719.
- [32] Y. Zhao, D.G. Truhlar, *Acc. Chem. Res.* 41 (2008) 157.
- [33] Y. Zhao, D.G. Truhlar, *Theor. Chem. Acc.* 120 (2008) 215.
- [34] F. Jensen, *J. Chem. Phys.* 115 (2001) 9113.
- [35] F. Jensen, T. Helgaker, *J. Chem. Phys.* 121 (2004) 3463.
- [36] P.Y. Ayala, H.B. Schlegel, *J. Chem. Phys.* 107 (1997) 375.
- [37] P. Jureka, P. Hobz, *Chem. Phys. Lett.* 365 (2002) 89.
- [38] M.O. Sinnokrot, C.D. Sherrill, *J. Phys. Chem. A* 108 (2004) 10200.
- [39] T.H. Dunning, *J. Chem. Phys.* 90 (1989) 1007.
- [40] D.E. Woon, T.H. Dunning, *J. Chem. Phys.* 98 (1993) 1358.
- [41] T. Helgaker, W. Klopper, H. Koch, J. Noga, *J. Chem. Phys.* 106 (1997) 9639.
- [42] A.J. Weldon, G.S. Tschumper, *Int. J. Quantum Chem.* 107 (2007) 2261.
- [43] A.J. Weldon, T.L. Vickerey, G.S. Tschumper, *J. Phys. Chem. A* 109 (2005) 11073.
- [44] F.A. Hamprecht, A. Cohen, D.J. Tozer, N.C. Handy, *J. Chem. Phys.* 109 (1998) 6264.
- [45] J.P. Merrick, D. Moran, L. Radom, *J. Phys. Chem. A* 111 (2007) 11683.
- [46] T. van Mourik, *J. Chem. Theory. Comput.* 4 (2008) 1610.
- [47] B. Andersen, H.M. Seip, T.G. Strand, R. Stolevik, *Acta Chem. Scand.* 23 (1969) 3224.
- [48] A.W. Ross, M. Fink, R.L. Hilderbrandt, *International Tables of Crystallography*, C. Kluwer Academic Publishers, Dordrecht, 1992.
- [49] V.A. Sipachev, *Vibrational effects in diffraction and microwave experiments: a start on the problem*, vol. 5, JAI Press, New York, 1999.
- [50] W.C. Hamilton, *Acta Cryst.* 18 (1965) 502.
- [51] H.F. Dos Santos, W.R. Rocha, W.B. De Almeida, *Chem. Phys.* 280 (2002) 31.
- [52] M.L. Franco, D.E. Ferreira, H.F. Dos Santos, W.B. De Almeida, *J. Chem. Theory. Comput.* 4 (2008) 728.